A Tunable 240–290 GHz Waveguide Enclosed 2-D Grid HBV Frequency Tripler

A Tunable 240–290 GHz Waveguide Enclosed 2-D Grid HBV Frequency Tripler

Robin Dahlbäck, *Student Member, IEEE*, Josip Vukusic, Robert M. Weikle II, *Senior Member, IEEE*, and Jan Stake, *Senior Member, IEEE*

***Abstract*—This paper presents a high-power 240–290 GHz waveguide enclosed two-dimensional (2-D) grid heterostructure barrier varactor (HBV) frequency multiplier. A 35 mW of output power is produced at 247 GHz with an input power of 900 mW. The operational bandwidth is tunable within a 50 GHz span by the use of an input tuner able to adjust the input matching of the 2-D grid HBV frequency multiplier. Tuning is achieved by moving a suspended dielectric slab in the input waveguide.**

***Index Terms*—Frequency multipliers, heterostructure barrier varactors (HBVs), impedance matching, quasi-optical, tuners, THz sources, varactors, 2-D grid.**

I. Introduction

THE growing number of applications for terahertz technology calls for ever increasing output power from signal sources [1]. The development of electronic-based sources and receivers at these frequencies has received considerable attention during the past decades [2]. Therefore, progress has recently been seen in emerging areas such as multipixel imaging [3], medical imaging [4], and millimeter wave imaging radars [5]. These applications benefit from higher transmitter powers for illumination of the test object in order to increase the frame rate or usable working distance. Similarly, frequency multiplier chains where the final output is high up in the THz band [6] or local oscillator sources driving multiple receivers benefit from high input power.

Due to the availability of watt level power, many THz multiplier chains start from a power amplifier at W-band, but such high pumping power [7] can be a challenge to handle for the first-stage multipliers. Therefore, a new generation of frequency multipliers capable of utilizing the increasing available power at around 100 GHz is becoming more important.

Two main strategies exist in the effort to increase the power handling of recent high-power frequency multipliers [8]–[10]. The first one is to increase the number of series or parallel coupled active devices on a chip, an approach that becomes more challenging as the operating frequency and number of active devices increase. The second approach, that usually follows the first, is to power combine many multiplier chips using split and combine waveguide networks. This method works well for a small number of chips but as the number of chips increases so do the losses in the waveguide network. Here, spatially power combined two-dimensional (2-D) grids have an advantage since the combining loss is independent of the number of devices [11]. Furthermore, 2-D grids can be built to be more compact than large waveguide combining networks.

Two-dimensional grid power combining has been successfully applied, for example, to amplifiers [11], oscillators [12], multipliers [13]–[15], and mixers [16]. Both free-space quasi-optical setups and waveguide enclosed spatially power combined 2-D grid designs have been demonstrated. A summary of state-of-the-art results in terms of output power from frequency multipliers operating in the 250–300 GHz range is given in Table I. Only continuous wave operation is considered, and the highest frequency waveguide enclosed 2-D grid result is included for reference.

The frequency multiplier module presented in Fig. 1 builds upon the work in [17] with the addition of an improved matching network in the form of an input matching tuner. The input tuner uses a movable dielectric slab in the input waveguide to optimize the input matching. Using this approach, we show significant improvements in operational bandwidth and conversion efficiency. The compact module presented here is to the authors' knowledge the first demonstration of this concept above 100 GHz.

II. Method

The multiplier 2-D grid module is based on a 72 element heterostructure barrier varactor diode (HBV [21]) tripler configured as 6×12 dipole unit cells. A cut through view of the complete module is shown in Fig. 1 and a photograph in Fig. 2.

The simulation model combines six parallel sets of equal cascaded unit cell models excited with different input powers. A combination of transmission line theory and numerical finite element frequency domain models is used to create the cascaded unit cell models as demonstrated in [22]. Periodic boundary conditions are imposed on the unit cells of the grid array and filter in Ansys HFSS that is used to calculate the scattering parameters. A transmission line representation of one of the cascaded unit cells is shown in Fig. 4. For initial estimations, a lump component model of the varactor unit cell calculated using the induced EMF method [23] was used instead of the finite-element model (FEM).

Manuscript received June 18, 2015; revised January 21, 2016; accepted March 7, 2016. This work was supported in part by the Swedish Research Council, VR, and in part by the European Space Agency, ESA.

R. Dahlbäck, J. Vukusic, and J. Stake are with the Terahertz and Millimetre Wave Laboratory, Department of Microtechnology and Nanoscience-MC2, Chalmers University of Technology, Göteborg SE-412 96, Sweden (e-mail: dahlback@chalmers.se; josip.vukusic@chalmers.se; jan.stake@chalmers.se).

R. M. Weikle II, is with the Charles L. Brown Department of Electrical and Computer Engineering, University of Virginia, Charlottesville, VA 22904 USA (e-mail: rmw5w@virginia.edu).

Color versions of one or more of the figures in this paper are available online at http://ieeexplore.ieee.org.

Digital Object Identifier 10.1109/TTHZ.2016.2545519

TABLE I
STATE-OF-THE-ART FREQUENCY MULTIPLIERS OPERATING IN THE 250–300 GHZ BAND

Technology	Output power	Efficiency	BW	Active devices	Input power	Power/device	Source	Comment
Schottky X2	53 mW at 286 GHz	–	5%	–	–	–	[18]	Diamond heat spreader
Schottky X2	40 mW at 240 GHz	11%	–	6	350 mW	58 mW	[19]	Diamond backed membrane
Schottky X2	27 mW at 300 GHz	7%	18%	6	408 mW	68 mW	[19]	Diamond backed membrane
Schottky X2	48 mW at 286 GHz	10%	–	–	500 mW	21 mW	[8]	Waveguide combiner
HBV X3	31 mW at 282 GHz	6%	4%	1 × 6 barriers	500 mW	500 mW	[20]	Monolithic integration
2-D grid HBV X3	684 mW at 93 GHz	10%	–	196 × 4 barriers	7000 mW	-	[15]	
2-D grid HBV X3	35 mW at 247 GHz	4%	3%	72 × 6 barriers	900 mW	24–0.6 mW		This paper, fix tuned

The highest power waveguide enclosed 2D-grid work is also included. For Schottky diodes each contact is counted as a device and for HBVs each mesa pair. BW represents the output power bandwidth and efficiency is the efficiency at peak output power. Some of the numbers are estimated from graphs.

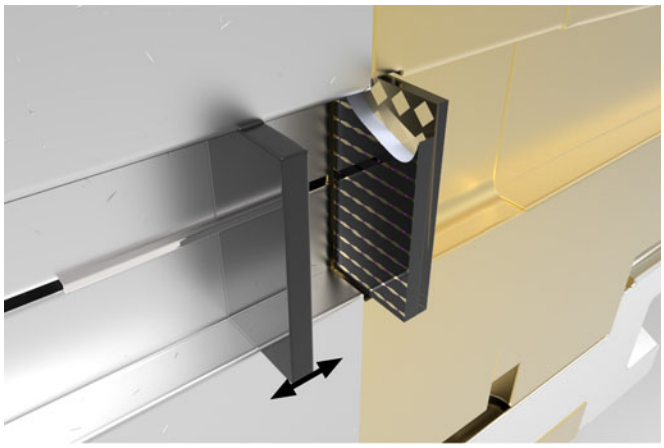

Fig. 1. Cut-through rendering showing the tuning slab, 2-D HBV grid and output filter inside the waveguide blocks. The arrow indicates tuning movement.

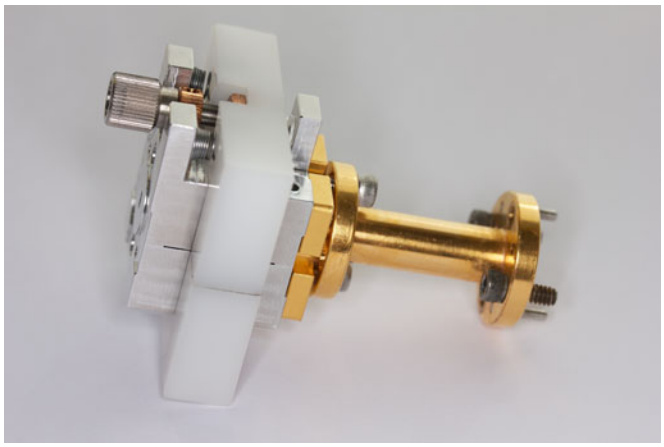

Fig. 2. Photograph of complete multiplier module. From left to right: Tuner assembly, shim housing the varactor array and finally the 25-mm long WR-10 to WR-03 linear waveguide taper.

The 2-D grid contains 72 unit cells but two assumptions in respect of symmetry are used to reduce the number of parallel unit cells in the simulation to six. First, the electrical symmetry of the input mode in the waveguide is used, see the dashed line in Fig. 3. Second, the contributions from elements in the same column are assumed to be identical. This results in six sets of identical unit cell models, of which one is shown in Fig. 4. Examples of their positions are marked with letters a–f in Fig. 3.

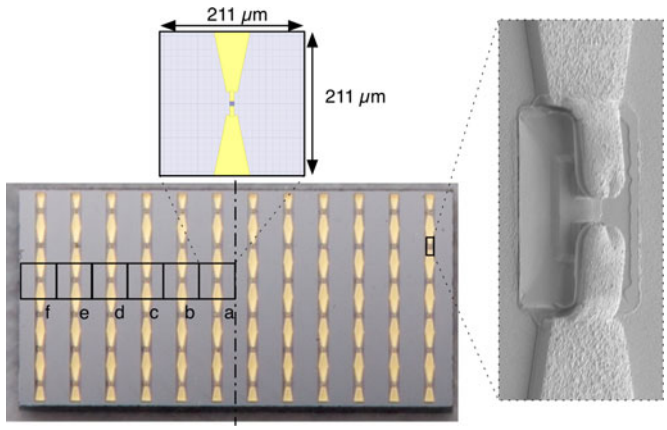

Fig. 3. Photograph of a fabricated HBV 2-D grid. The squares labeled a–f indicate the positions of the unit cells used in the model and the dashed line indicates the electrical symmetry. Top left: Unit cell dimensions. Right: SEM picture of one of the HBV diodes, consisting of two mesas.

A. *Effects of Nonuniform Excitation*

The input H_{10} mode power density is used to estimate the drive levels of the unit cells a–f; the results are given in Table II. The unit-cell models are assumed to be driven in phase, although due to the different drive levels, the third harmonic outputs will be out of phase. Fig. 9 shows two estimates of the conversion efficiency, denoted as scalar summed efficiency and vector summed efficiency. For the scalar summed efficiency, the output power values from the six unit cells are summed and then divided by the total input power to the unit cells. In the vector summed efficiency, the unit cells are power combined in the simulation software, thus accounting for the phase difference at the outputs.

Due to the uneven input power distribution, the conversion efficiency of the columns a–f will differ. The individual unit cell conversion efficiencies are presented in Table II. The circuit is tuned for maximum output power at each input power point, i.e., maximum vector summed efficiency.

B. *Device Failures*

One potential advantage of 2-D grid power combining is the resilience against catastrophic failure caused by single device failures. The first-order approximation for device failures in the 2-D grid assumes that only the contribution of the failed

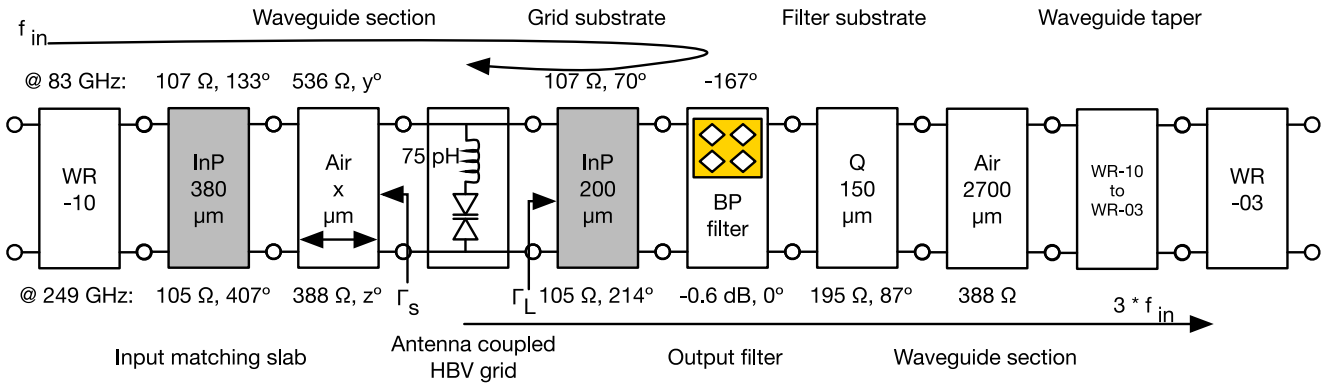

Fig. 4. Unit-cell transmission line model of the multiplier module. The variable source impedance, Γ_s, presented to the tripler 2-D grid by the tuner is also indicated. The multiple functions of the output filter stack are also explained by the arrows indicating the wave paths through the network. Note the 75 pH lump inductor that was used as an initial model for the 2-D grid unit cell antenna.

TABLE II
DISTRIBUTION OF INPUT POWER AND CONVERSION EFFICIENCY AMONG THE UNIT-CELL MODELS CORRESPONDING TO THE COLUMNS A–F

	Unit Cell Input Power						
Input power	a	b	c	d	e	f	Unit
Relative	1	0.87	0.64	0.38	0.15	0.02	–
100 mW	2.7	2.4	1.7	1.0	0.4	0.06	mW
500 mW	14	12	8.7	5.2	2.1	0.31	mW
900 mW	24	21	16	9.3	3.8	0.56	mW
	Conversion efficiency						
Input power	a	b	c	d	e	f	Unit
100 mW	4.3	4.1	3.2	1.3	0.13	0	%
500 mW	9.7	10	11	10	0.4	0	%
900 mW	17	18	19	0.3	0.04	0	%

Examples are given for three module input powers.

TABLE III
REDUCTION OF THE TOTAL OUTPUT POWER IF THE CONTRIBUTION FROM ONE SINGLE UNIT CELL FROM COLUMNS A TO F OR THEIR MIRROR COPY FAILS

Input power	a	b	c	d	e	f	Unit
100 mW	−3.2	−3.1	−2.3	−0.15	0.15	0	%
500 mW	−2.7	−2.7	−2.5	−0.6	0.02	0	%
900 mW	−3.1	−3.1	−2.2	−0.06	−0.03	0	%

Examples are given for three module input powers and the tuning distance is set for maximum output power at 247 GHz.

device to the output power is lost. This does not account for how a failed device affects the neighboring devices' embedding impedance and, therefore, the assumption must be used with caution. It may however give a good estimate of the contribution from every cell to the output power for a fully functional array. Using the above assumption, the result in Table III was calculated. The table shows that the three unit cell columns on each side of the center symmetry line contribute almost all of the output power.

III. DESIGN

The multiplier module from input to output consists of a 380 µm thick (approximately λ/4) InP matching slab that can be moved by the tuner, the dipole array on the 200 µm varactor substrate and a bandpass filter surface on 150 µm quartz. The outer array dimensions are 2.54 × 1.27 mm^2, thus matching a standard WR-10 waveguide. Varactors, matching slab, and filter were all fabricated by the authors in the Chalmers Nanofabrication Laboratory. The filter and varactor stack are mounted in a 3-mm-thick WR-10 waveguide shim. A 200-µm-deep pocket extending 100 µm outside the waveguide is housing the array and filter stack. A WR-10 to WR-3 linear taper is used to secure a fundamental H_{10} mode interface on the output.

A. 2-D Varactor Grid Design

The design of a 2-D grid varactor multiplier is a multivariable problem with many dependencies. To reduce the number of variables, the initial design constrains listed below were used:

1) All unit cells are identical.
2) Square unit cells.
3) An even number of unit cell rows and columns.
4) The conditions defined above ensure the symmetry drawn as a dashed line in Fig. 3.
5) Design for 1 W of input power.
6) HBVs based on the epitaxial material presented below.

The HBVs used are two mesa devices with the same epitaxial design as presented in [24] but with three barriers. The modeling equations used for the harmonic balance simulations are described in [25]. Iterative thermal and electrical simulations resulted in using a 20 µm^2 two mesa HBV in a 6 × 12 grid with dipole like antennae. In the simulation model, a series resistance of 21 Ω and breakdown voltage of 33 V was used. Power handling capacity, conversion efficiency, and matching are the parameters considered in the design. HBV optimization was done using a combination of three dimensional (3-D) FEM models to predict heat transport and harmonic balance simulations for the electrical performance.

B. Filter Design

The filter (shown in Fig. 5) is implemented as a rhombic aperture frequency selective surface, fabricated by plating of

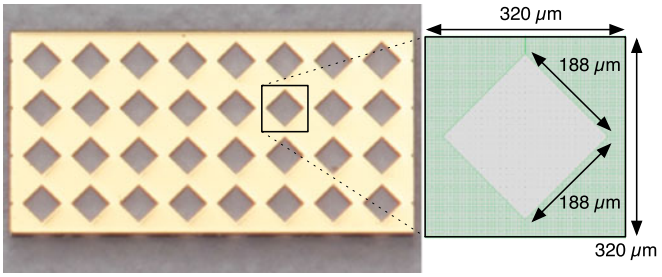

Fig. 5. Photograph of the bandpass filter. Four by eight 320 μm square unit cells make up the filter. The side dimensions of the rhombic apertures are 188 μm.

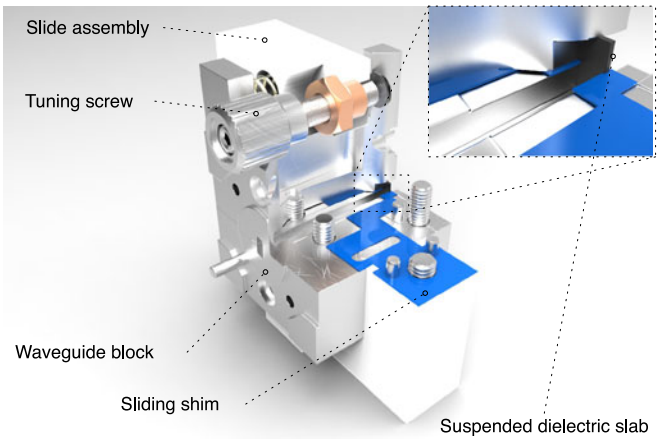

Fig. 6. Cut-through rendering of the complete tuner. The sliding steel shim is colored blue to improve visibility.

1.5-μm gold on a 150-μm quartz substrate. It serves as a backshort for the input pump frequency. At the output third harmonic, it provides a bandpass response and the filter substrate acts as a λ/4 transformer matching the propagating third harmonic to the output waveguide. The filter also transfers heat to the metal housing due to the direct contact with the array substrate.

Since two different power amplifiers were available as test sources, the filter was designed to have pass bands corresponding to each of the amplifiers (centered at 82 and 93 GHz). The dual pass bands are a tradeoff to minimize insertion loss, where the amplifiers peak in power. This design is simulated to give a stable reflection phase of approximately π and a pass band loss of 0.6 dB at 249 GHz. An important consideration is that the response is dependent on the embedding impedance of the InP substrate on one side and the quartz substrate on the other side. Simulated S_{21} results for the unit-cell filter model are plotted in Fig. 8.

C. Tuner Design

The tuner presented in Fig. 6 uses a movable dielectric slab, functioning as a low-impedance transmission line. The embedding impedance seen on the multiplier's input side (Γ_S in Fig. 4) can thus be tuned by varying the length of the air filled part, see Fig. 1 for a detail view. A 380-μ*m*-thick InP substrate fitting

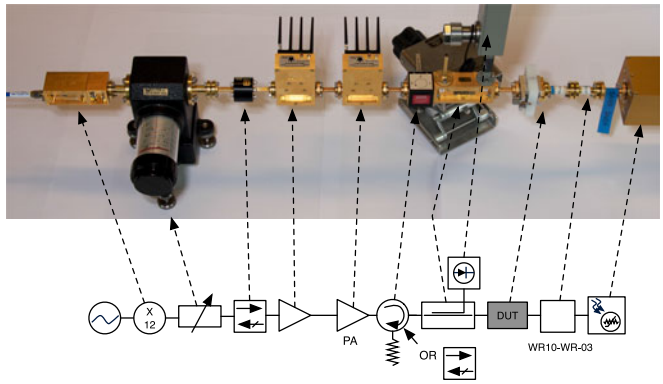

Fig. 7. Photograph of the measurement setup together with a block schematic diagram. The frequency synthesizer is not present in the picture and the amplifier bias cables are also removed to reduce clutter.

inside the WR-10 waveguide, equivalent to a 107 Ω, 133 ° long transmission line at 83 GHz is used as a tuning element. In Fig. 1, the tuning slab, 2-D HBV grid, and output filter are shown inside the waveguide blocks.

The mechanical design is utilizing the fact that no current is flowing in the waveguide wall across the E-plane symmetry line (when excited with the H_{10} mode). A thin slit in the waveguide wall can thus be made without significantly affecting the propagating field. The tuning slab is held in place by a stainless steel shim extending into the waveguide through the slit. Clamped to the outer surfaces of the waveguide block is a sliding positioning fixture made from low friction polyoxymethylene machine plastic. A fine-pitch tuning screw is used to move the sliding fixture, steel shim, and tuning slab along the waveguide's propagation direction. This design allows a tuning range of a few millimeters (equivalent to more than λ/2 at the input frequency) in precise steps with a minimum distance between the tuning substrate and the varactor array surface of approximately 0.2 mm.

IV. Measurements

A schematic diagram together with a photograph of the measurement setup is shown in Fig. 7. Two different GaN power amplifiers were used to drive the multiplier module. The amplifiers have operating bands centered at 82 GHz (Wasa Millimeter Wave WPA-108227) and 93 GHz (Wasa Millimeter Wave WPA-10-932714).

A microwave synthesizer (Keysight E8257D) is used to generate the test signal driving the X12 frequency multiplier module (Custom from Wasa Millimetre Wave). Following the multiplier module is a direct reading attenuator (Millitech DRA-10) and a full band isolator (Millitech FBI-10). A broadband preamplifier (Wasa Millimeter Wave WPA-10-882015) then drives either of the two power amplifiers. The output from the power amplifier is isolated from the device under test by a circulator (Millitech JFD-10) at the lower 83 GHz band and by a full band isolator (Millitech FBI-10) at the higher 93 GHz band. During the measurement, the forward power to the module is continuously monitored using a waveguide coupler (Millitech CE4-10) and

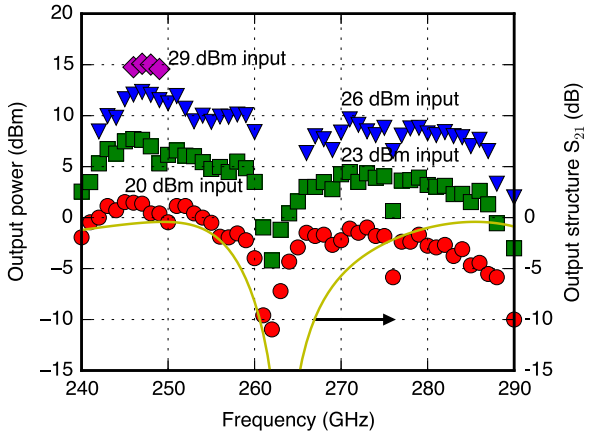

Fig. 8. Measured output power as a function of frequency and input power. Input power is marked in the graph next to the data series. The tuner reached the end position at the higher frequency limit. Simulated unit-cell filter structure (from the InP varactor substrate to the Quartz filter substrate) S_{21} response is also included as solid line.

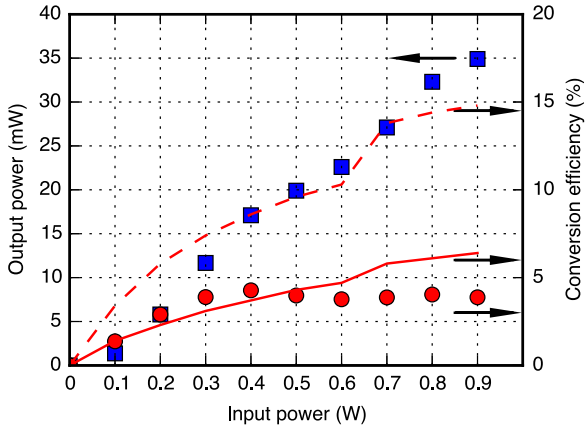

Fig. 9. Measured output power (blue squares) and conversion efficiency (red circles) as a function of input power at 247 GHz. Simulated scalar summed efficiency (dashed line) and vector summed efficiency (solid line) are also plotted.

a calibrated waveguide power sensor (Keysight W8486A). The output power is measured using a calorimetric power sensor (VDI - Erickson PM4) connected through a 1″ WR-10 waveguide section and a WR-10 to WR-03 linear taper.

No compensation of the measured power is done for the losses in the waveguide taper or the straight section. It is estimated that these components cause approximately 0.6 dB of loss [26].

The measured output power as a function of the frequency and the input power is plotted in Fig. 8. For each measurement point, the tuner is adjusted to yield the maximum output power. The dip in the middle of the frequency span corresponds well to the design of the output filters S_{21}, drawn as a solid line in the plot. The maximum output power measured was 35 mW at 247-GHz output frequency with 900 mW of pump power. At 247 GHz the conversion efficiency peaked at 4.3% with 400 mW of pump power. The use of two different amplifiers explains the lack of available test power in the center of the measurement band.

The tuned output power and conversion efficiency as a function of the input power at 247 GHz is plotted in Fig. 9. Overlaid are also the simulated scalar and vector summed conversion efficiencies from Section III-A.

To illustrate the effect of tuning, a comparative plot is shown in Fig. 10. Here, the module is tuned at 251 GHz and 500 mW input power. The figure shows the difference between the tuning point and the continuously tuned data in Fig. 8.

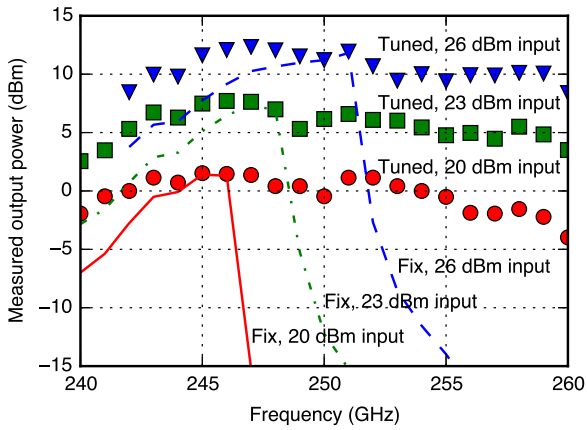

Fig. 10. Discrete points (triangles, squares, and circles) represent continuously tuned output power with three different input powers. The lines are the measured data when the tuner is set to maximum output power at 251 GHz with 27 dBm input power.

V. Discussion

The vector summed efficiency in Fig. 9 is in reasonable agreement with the measured data. At high input powers (above 600 mW) the deviation increases. One possible explanation is self-heating effects [27] not included in the model or higher mode excitation as discussed below. The scalar summed efficiency is in general approximately twice the calculated vector summed or measured efficiency. This indicates that the different phase of the output third harmonic at different positions in the array is responsible for a 3-dB reduction in output power. In Table III are the data indicating that at 100 and 500 mW input power column e also degrades the total output power, since the column's third harmonic power is adding out of phase. Future design attempts should aim to reduce this effect.

The fix tuned case presented in Fig. 10 has a peak in conversion efficiency that varies with input power. This comes from the fact that the average capacitance of the varactors is dependent on input power and thus this behavior is typical for varactor frequency multipliers.

The potential problem with output power in other modes than the fundamental H_{10} has not been carefully investigated in this paper. A method of estimating the mode content in the output has been presented in [14]. The differences in conversion efficiency between the columns will result in excitation of higher order modes at the output. The uneven conversion efficiency between the different columns, particularly at high-drive levels may explain the increasing difference between modeled and measured conversion efficiency.

In order to minimize ohmic losses in the input network no frequency selective metal surface is used to stop the third harmonic from propagating toward the input. Instead the output coupling relies on the impedance presented to the 2-D grid by the input and output network, Γ_{S} and Γ_{L} in Fig. 4. A consequence is that it is hard to design a broadband matching, but this is partially compensated for by the use of the tuner. The input match and output power of the multiplier without the matching slab is quite poor. During experiments without the tuner, the peak output power is reduced to approximately 1 mW and the input VSWR > 10. When tuned for maximum output power, the VSWR on the input is reduced to approximately 2. One potential disadvantage with the tuner is that a slight tilt of the tuning substrate may excite substrate modes causing strong resonances in the input network.

Due to the different matching conditions that are available, it is difficult to predict the maximum power handling capacity of the module. The available input power of 900 mW has not been enough to destroy the varactor grid. Simulations indicate that electric breakdown can occur in the center columns at powers above 1 W under certain tuning conditions. However, if the center columns are slightly detuned, simulations indicate that operation at higher input power is possible. The main thermal limitation is heat transport from the mesa to the substrate, limited by the InGaAs epi-layers [28]. The thermal simulations predict a maximum absorbed power of 40 mW per device, which if all incident power is assumed to be absorbed occurs for the center columns at approximately 1.5 W of input power. Altogether, it is hard to determine the maximum usable input power without destructive experiments; there is no success like failure.

Having an in band transmission zero in the output filter (model S_{21} plotted in Fig. 8) may not be optimal for the complete module performance, however, it is useful to verify the modeling approach. The resonance frequency of the filter embedded in the waveguide corresponds to the unit-cell design to within 1%. This further supports the usability of unit cell modeling of relatively small arrays enclosed inside metal waveguides.

The shim system used to mount the array is forgiving in terms of manufacturing dimensions, complexity, and tolerances. For a fix tuned version, an equally simple shim could be manufactured to hold the input matching slab. Branch guide couplers at 300 GHz, typically implemented in waveguide-based power combining circuits, may require fabrication tolerances in the order of 10 μm and high aspect ratio end mills. The shim system used here can accept mechanical tolerances in the order of 100 μm.

VI. Conclusion

A tunable 240–290 GHz waveguide enclosed 2-D grid HBV frequency tripler has been designed and characterized experimentally.

Peak conversion efficiency of 4.3% is achieved with 400 mW of input power at 247 GHz. A tuner enables tuning of the inherently narrowband varactor circuit over an 18% relative bandwidth. This is to the authors' knowledge the highest frequency waveguide embedded 2-D grid frequency multiplier presented to date.

A modified version of unit-cell modeling accounting for differences in input power and output phase is successfully applied. Future work will focus on improving the 2-D grids for even higher power handling and conversion efficiency. A key aspect will be even out the differences in output phase and conversion efficiency between the unit cells. This could possibly be achieved either by creating a more even excitation, by using nonuniform unit cells or HBVs of different sizes.

Another goal is the development of a full 3-D model design approach, where all the nonlinear elements are simulated, together with a complete FEM of the complete grid and filter stack in the waveguide environment. This would account for edge effects and evanescent mode coupling between the elements. Accurate modeling of different types of failure scenarios would also be possible. These simulations are atleast an order of magnitude more time-consuming than the approach employed here and may therefore be most useful for final design verifications as a complement to simpler models.

The concept presented in this paper is scalable in terms of higher power handling for future THz sources.

Acknowledgment

The authors would like to thank Mr. Carl-Magnus Kihlman at Chalmers University, Sweden, for machining the waveguide components and Dr. T. Närhi at ESA for helpful discussions. Mr. G. Hrubó, is appreciated for helpful discussions about simulation models and Mr. V. Drakinskiy for help with processing issues. Furthermore, the authors thank Wasa Millimeter Wave for lending them the power amplifiers used for testing.

References

[1] G. Chattopadhyay, "Technology, capabilities, and performance of low power terahertz sources," *IEEE Trans. THz Sci. Technol.*, vol. 1, no. 1, pp. 33–53, Sep. 2011.

[2] P. Siegel, "Terahertz technology," *IEEE Trans. Microw. Theory Techn.*, vol. 50, no. 3, pp. 910–928, Mar. 2002.

[3] R. Al Hadi *et al.*, "A 1 k-pixel video camera for 0.7–1.1 terahertz imaging applications in 65-nm CMOS," *IEEE J. Solid-State Circuits*, vol. 47, no. 12, pp. 2999–3012, Dec. 2012.

[4] C. Yu, S. Fan, Y. Sun, and E. Pickwell-MacPherson, "The potential of terahertz imaging for cancer diagnosis: A review of investigations to date," *Quantitative Imag. Med. Surg.*, vol. 2, pp. 33–45, 2012.

[5] K. B. Cooper, R. J. Dengler, N. Llombart, B. Thomas, G. Chattopadhyay, and P. H. Siegel, "THz imaging radar for standoff personnel screening," *IEEE Trans. THz Sci. Technol.*, vol. 1, no. 1, pp. 169–182, Sep. 2011.

[6] A. Maestrini *et al.*, "Design and characterization of a room temperature all-solid-state electronic source tunable from 2.48 to 2.75 THz," *IEEE Trans. THz Sci. Technol.*, vol. 2, no. 2, pp. 177–185, Mar. 2012.

[7] J. Schellenberg, E. Watkins, M. Micovic, B. Kim, and K. Han, "W-band, 5W solid-state power amplifier/combiner," in *Proc. IEEE MTT-S Int. Microw. Symp. Dig.*, 2010, pp. 240–243.

[8] A. Maestrini *et al.*, "A frequency-multiplied source with more than 1 mW of power across the 840–900-GHz band," *IEEE Trans. Microw. Theory Techn.*, vol. 58, no. 7, pp. 1925–1932, Jul. 2010.

[9] J. V. Siles *et al.*, "A high-power 105–120 GHz broadband on-chip power-combined frequency tripler," *IEEE Microw. Wireless Compon. Lett.*, vol. 25, no. 3, pp. 157–159, Mar. 2015.

[10] N. Alijabbari, M. F. Bauwens, and R. M. Weikle, "160 GHz balanced frequency quadruplers based on quasi-vertical Schottky varactors integrated on micromachined silicon," *IEEE Trans. THz Sci. Technol.*, vol. 4, no. 6, pp. 678–685, Nov. 2014.

[11] M. P. DeLisio and R. York, "Quasi-optical and spatial power combining," *IEEE Trans. Microw. Theory Techn.*, vol. 50, no. 3, pp. 929–936, Mar. 2002.

[12] Z. B. Popovic, R. M. Weikle II, M. Kim, and D. B. Rutledge, "A 100-MESFET planar grid oscillator," *IEEE Trans. Microw. Theory Techn.*, vol. 39, no. 2, pp. 193–200, Feb. 1991.
[13] A. Moussessian *et al.*, "A terahertz grid frequency doubler," *IEEE Trans. Microw. Theory Techn.*, vol. 46, no. 11, pp. 1976–1981, Nov. 1998.
[14] S. A. Rosenau, "Quasi-optical overmoded waveguide frequency multiplier grid arrays," Ph.D. Dissertation, Dept. Elect. Comput. Eng., Univ. California Davis, Davis, CA, USA, 2001.
[15] J. B. Hacker, A. L. Sailer, B. Brar, G. Nagy, R. L. J. Pierson, and J. A. Higgins, "A high-power W-band quasi-optical frequency tripler," in *Proc. IEEE MTT-S Int. Microw. Symp. Dig.*, 2003, vol. 3, pp. 1859–1862.
[16] J. B. Hacker, R. M. Weikle II, M. Kim, M. P. DeLisio, and D. B. Rutledge, "A 100-element planar Schottky diode grid mixer," *IEEE Trans. Microw. Theory Techn.*, vol. 40, no. 3, pp. 557–562, Mar. 1992.
[17] R. Dahlback, J. Vukusic, J. Stake, and R. M. Weikle, "A waveguide embedded 250 GHz quasi-optical frequency-tripler array," in *Proc. 44th Eur. Microw. Conf.*, 2014, pp. 802–805.
[18] T. W. Crowe, J. L. Hesler, and S. A. Retzloff, "Solid-state LO sources for greater than 2THz," presented at Int. Symp. Space THz Technology, Tucson, AZ, USA, Apr. 2011.
[19] C. Lee *et al.*, "A wafer-level diamond bonding process to improve power handling capability of submillimeter-wave Schottky diode frequency multipliers," in *Proc. IEEE MTT-S Int. Microw. Symp. Dig.*, 2009, pp. 957–960.
[20] J. Vukusic, J. Stake, T. Bryllert, Ø. Olsen, and J. Hanning, "Monolithic HBV-based 282-GHz tripler with 31-mW output power," *IEEE Electron. Device Lett.*, vol. 33, no. 6, pp. 800–802, Jun. 2012.
[21] E. Kollberg and A. Rydberg, "Quantum-barrier-varactor diodes for high efficiency millimetre-wave multipliers," *Electron. Lett.*, vol. 25, no. 25, pp. 1696–1698, 1989.
[22] W. A. Shiroma, S. C. Bundy, S. Hollung, B. D. Bauernfeind, and Z. B. Popovic, "Cascaded active and passive quasi-optical grids," *IEEE Trans. Microw. Theory Tech.*, vol. 43, no. 12, pp. 2904–2909, Dec. 1995.
[23] R. M. Weikle II, "Quasi-optical planar grids for microwave and millimeter-wave power combining," Ph.D. dissertation, Dept. Elect. Eng., California Inst. Technol., Pasadena, CA, USA, 1992.
[24] T. A. Emadi, J. Stake, T. Bryllert, M. Sadeghi, and J. Vukusic, "Optimum barrier thickness study for the InGaAs/InAlAs/AlAs heterostructure barrier varactor diodes," *Appl. Phys. Lett.*, vol. 90, no. 1, 2007, Art. no. 012108.
[25] L. Dillner *et al.*, "Frequency multiplier measurements on heterostructure barrier varactors on a copper substrate," *IEEE Electron. Device Lett.*, vol. 21, no. 5, pp. 206–208, May 2000.
[26] Virginia Diodes Inc. (2007, Dec.) VDI application note power measurement above 110 GHz [Online]. Available: http://vadiodes.com/
[27] M. Ingvarson, J. Vukusic, A. Olsen, T. A. Emadi, and J. Stake, "An electrothermal HBV model," in *Proc. IEEE MTT-S Int. Microw. Symp. Dig.*, 2005, pp. 1151–1153.
[28] M. Ingvarson, B. Alderman, A. O. Olsen, J. Vukusic, and J. Stake, "Thermal constraints for heterostructure barrier varactors," *IEEE Electron Device Lett.*, vol. 25, no. 11, pp. 713–715, Nov. 2004.

Robin Dahlbäck (S'10) received the M.Sc. degree in electrical engineering from the Chalmers University of Technology, Göteborg, Sweden, in 2010. He is currently working toward the Ph.D. degree at the Terahertz and Millimetre Wave Laboratory, Chalmers University of Technology.

His research interests include high-power THz solid state sources, system design, and THz imaging.

Josip Vukusic received the Diploma and Ph.D. degrees in photonics from the Chalmers University of Technology, Göteborg, Sweden, in 1997 and 2003, respectively.

He has been with the Terahertz and Millimetre Wave Laboratory, Department of Microtechnology and Nanoscience, Chalmers University of Technology, since 2004, where he is involved with terahertz technology. He is currently involved in the modeling, fabrication, and characterization of frequency multipliers for terahertz generation.

Robert M. Weikle, II (S'90–M'91–SM'05) was born in Tacoma, WA, USA, in 1963. He received the B.S. degree in electrical engineering and physics from Rice University, Houston, TX, USA, in 1986 and the M.S. and the Ph.D. degrees in electrical engineering from the California Institute of Technology, CA, USA, in 1987 and 1992, respectively.

Since 1993, he has been with the faculty of the University of Virginia, Charlottesville, VA, USA, where he is currently a Professor in the Department of Electrical and Computer Engineering. His research group focuses on submillimeter electronics, terahertz devices, high-frequency instrumentation and metrology, and quasi-optical techniques for millimeter-wave power combining and imaging.

Jan Stake (S'95–M'00–SM'06) was born in Uddevalla, Sweden, in 1971. He received the M.Sc. degree in electrical engineering and the Ph.D. degree in microwave electronics from the Chalmers University of Technology, Göteborg, Sweden, in 1994 and 1999, respectively.

In 1997, he was a Research Assistant with the University of Virginia. From 1999 to 2001, he was a Research Fellow with the Millimetre Wave Group, Rutherford Appleton Laboratory, Didcot, U.K. Till 2003, he was a Senior RF/Microwave Engineer with Saab Com-bitech Systems AB. From 2000 to 2006, he held different academic positions with Chalmers University of Technology and, from 2003 to 2006, was also the Head of the Nanofabrication Laboratory, Department of Microtechnology and Nanoscience (MC2). During summer 2007, he was a Visiting Professor with the Submillimeter Wave Advanced Technology Group, Caltech/JPL, Pasadena, CA, USA. He is currently a Professor and the Head of the Terahertz and Millimetre Wave Laboratory, Chalmers University of Technology, Sweden. He is also cofounder of Wasa Millimeter Wave AB, Göteborg, Sweden. His research interests include graphene electronics, high-frequency semiconductor devices, THz electronics, submillimeter wave measurement techniques (ÄúTHz metrology ,Äù), and THz in biology and medicine.

Prof. Stake serves as the Editor-in-Chief for the IEEE TRANSACTIONS ON TERAHERTZ SCIENCE AND TECHNOLOGY.